Steel to aluminium braze-welding by laser process with and Al-12Si filler wire

Guillaume Sierra, Patrice Peyre, Frédéric Deschaux-Beaume, David Stuart, Gilles Fras

Steel to aluminium braze welding by laser process with Al–12Si filler wire

G. Sierra[1,2], P. Peyre[3], F. Deschaux Beaume*[2], D. Stuart[3] and G. Fras[2]

The joining of DC04 steel to 6016-T4 Al alloy is achieved by laser braze welding using a 4047 (Al–12Si) filler wire and a brazing flux. The dissimilar joining is obtained both by welding the parent 6016 alloy to the 4047 filler wire, producing a continuous bonding without apparent macroscopic flaws, and by reactive wetting of the molten Al alloy on the solid steel, resulting in the formation of a thin layer of Fe–Al–Si intermetallic compounds at the steel/bead interface. The linear strength of the assemblies can be as high as 190 N mm21, with a failure generally located in the reaction layer of the steel/bead interface. Last, the strength of the assemblies is shown to increase linearly with the reaction layer width.

Keywords: Al alloys, Steel, Interfaces, Braze welding, Intermetallic compounds, Dissimilar joining

Introduction

In the next few years, the automotive industry will aim to reduce vehicle fuel consumption in order to meet the new antipollution standards. This objective may be reached by lightening the vehicles; that is why nowadays several manufacturing methods combining the use of high strength steels and light alloys like Al or Mg alloys are being investigated. Manufacturing cars using steel and light alloys implies the joining of dissimilar materials. However, the welding of steel to Al still remains a technological issue, due to the great difference in the physical properties of both materials (melting temperature, thermal expansion coefficient, etc.) and most of all because of the near zero solid solubility of iron in Al, resulting in the formation of brittle intermetallic compounds.

Several methods of joining steel to Al have already been investigated, involving solid state joining,[1–5] reactive wetting (interaction between solid steel and liquid Al)[6–18] or laser key hole welding.[19,20] The steel to Al solid state joining was studied using various processes, such as explosion welding,[1] friction welding,[2,3] and more recently friction stir welding.[4,5] Classical welding processes such as arc welding,[6,7] resistance spot welding[8,9] and brazing[10] were used to develop a solid steel to liquid Al joining. Nevertheless, the major work of these last years has been the development of the laser process. Taking advantage of the high welding velocity of the process and of the resulting limited interaction times, liquid steel to liquid Al interaction by key hole mode[18–20] was investigated, with some interesting results. However, the best results were achieved by laser reactive wetting, involving an Al induced melting by heat conduction through the steel,[11,12] and more recently by direct laser melting of Al.[17,18] Authors[13–16,18] have also used filler wires with low melting temperature to limit the energy input to the assembly in order to reduce steel/Al interfacial temperature. This 'braze welding' technique involves welding between the parent Al alloy and the filler wire, and brazing between liquid filler wire and solid steel. Braze welding of Al alloy and galvanised steel using Al–12Si filler wire (4047 alloy) has been studied,[12,13] in order to verify the beneficial effect of Si on the growth kinetic of Fe–Al intermetallics.[21] A Zn–Al filler wire has also been used,[14,15] enabling the realisation of dissimilar steel/Al joints without brazing flux. Owing to the promising mechanical strengths obtained by laser braze welding, this technique was also carried out by Metal Inter Gas (MIG) process in a lap configuration.[6,7]

In all previous studies, whatever the process, steel to Al joining has been ensured by the formation of intermetallic phases predicted by the Fe–Al equilibrium diagram. In turn, the main issue concerning the steel/Al assembling comes from the rapid formation of these phases and their extremely brittle mechanical behaviour. This usually results in a brittle fracture of these interfacial phases.

The aim of the present work is to confirm the results obtained on laser braze welding of non-galvanised steel to Al, using an Al–12Si filler wire,[16] and to compare them with previous results obtained by reactive wetting.[17] The assemblies were studied following a metallurgical and mechanical approach, with a special focus on the intermetallic reaction layers and the strength of the assemblies. Finally, the mechanical results were compared to previous results obtained by reactive wetting on non-galvanised steels.[18]

[1]CEA/DRT/DTEN/LITEN/UTIAC, Groupement d'Etudes et de Recherche pour l'Application Industrielle des Lasers de Puissance (GERAILP), 94114 Arcueil, France
[2]Laboratoire de Mécanique et Génie Civil, UMR 5508 CNRS, Université Montpellier II, 34095 Montpellier, France
[3]GIP-GERAILP, Laboratoire pour l'Application des Lasers de Puissance, UPR 1578 CNRS, 94114Arcueil, France

*Corresponding author, email deschaux@iut-nimes.fr

Materials

The base materials used for these investigations are a low carbon steel DC04, defined by the European normalisation EN 10130, and a 6016-T4 Al alloy respectively provided as 1·2 and 1 mm thick sheets. A 4047 Al alloy (Al–12Si) is used as brazing material, in the form of a 1 mm diameter filler wire. This alloy is currently used for Al alloys brazing, because it has low melting temperature (577°C) resulting from its Al–Si nearly eutectic composition. The chemical compositions and mechanical properties of the materials are given in Tables 1 and 2 respectively.

An anticorrosive brazing flux Nocolok (Solvay Fluor GmbH) is deposited on the base materials before joining, in order to remove Al and steel oxides and prevent the oxidation of Al during its melting. This Al potassium fluoride flux ($K_{1-3}AlF_{4-6}$) is well suited to the brazing of Al alloys, because its melting temperature is in the 565–572°C range, just below the melting temperature of the 4047 alloy. The liquid flux can then dissolve the surface oxides just before the Al melts, and allow it to spread.

Experimental

Braze welding experiments

The braze welding tests are carried out on two 120 × 90 mm Al and steel sheets, in a lap configuration, the Al sheet being upon the steel one (Fig. 1*a*). The sheet surface is prepared by grade 800 SiC polishing, and degreased with acetone before assembling. A suspension of brazing flux in ethanol is sprayed on the steel surface, and dried before assembling to obtain an average flux thickness of 30 ± 20 μm.

Lap braze welding tests are carried out with a Nd:YAG continuous wave laser operating in the 2–2·5 kW power range, with scanning speeds of 1 m min^{-1}. The 1 mm filler wire is unwound at a speed of 2–3 m min^{-1}. Operating with a 200 mm focal lens, laser is used in defocused condition, with a 30° irradiation angle, resulting in an elliptic spot of 1·8 × 1·5 mm, and laser intensities of 70–90 kW cm^{-2} (Fig. 1*a*).

The laser beam irradiates directly both the filler wire and the upper Al sheet (Fig. 1*b*). Preliminary tests made it possible to define the optimal position of the laser beam towards the filler wire and the Al sheet. The heated surfaces are protected from oxidation by an argon shielding gas nozzle at nearly 10 L min^{-1}.

For each assembly, a fast camera (C-mos 4000 Hz) recording of the melt pool (Fig. 1*a*) is used to observe the melting and mixture of parent Al alloy and filler wire, with the objective of stabilising the melt pool and optimising the process conditions.

Table 1 Chemical composition of materials, wt-%

Element	Al	Fe	Mg	Si	Cu	Mn	P+S	C
DC 04	–	Bal.	–	–	–	0·4	0·06	0·08
6016	Bal.	0·5	0·3–0·5	1–1·3	0·2	0·2	–	–
4047	Bal.	0·2		12·0				

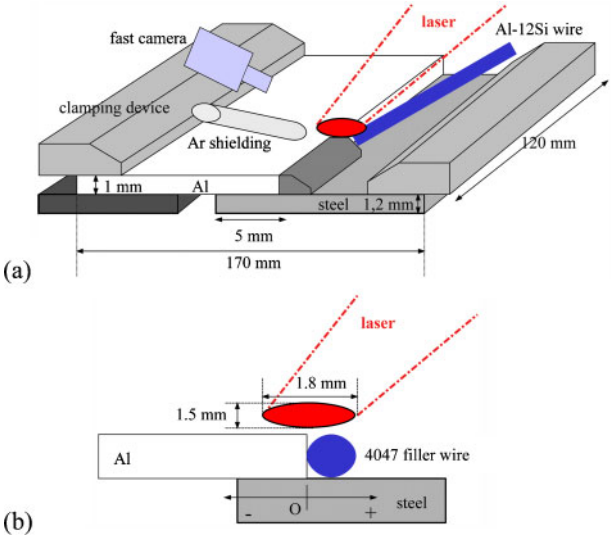

1 *a* schematic description of experimental set-up used for braze welding tests and *b* laser spot location towards 4047 and 6016 alloys

Metallurgical and mechanical characterisations

Cross-sections are cut in the braze welded samples, and then polished to obtain a mirror-like surface, before etching with Keller's reagent and nital to reveal the microstructures of Al and steel respectively.

The cross-sections of the joints are examined using optical microscopy, scanning electron microscopy (SEM) with an energy dispersive X-ray (EDX) analysis, and electron probe microanalysis (EPMA).

For each welding condition, three transverse tensile test specimens (120 × 20 mm) are machined from the assemblies. Tensile tests are achieved at a constant travel speed of 1 mm min^{-1}, with a loading direction perpendicular to the joining line (Fig. 2). Finally, the fracture surfaces of the specimens were analysed by SEM to try to identify the fracture path.

Macroscopic and microstructural analyses

Optimisation of braze welding parameters

The bonding quality is widely dependent on the operating parameters, and particularly on the relative position of the laser spot, the Al sheet, and the filler wire. More precisely, if the laser beam does not allow the full melting of the parent Al, the joining between the melted filler wire and the Al sheet is not achieved on the whole Al thickness (Fig. 3*a*), as previously observed by Saida.[16]

In order to optimise the locations of the laser spot and the filler wire, fast camera video recording were carried out and analysed. Figure 4*a* shows a 2000 image per second recording of the beginning of the filler wire melting, with optimised parameters (one-third of the beam diameter directed on the sheet and two-thirds on the wire). One can clearly observe the simultaneous

Table 2 Mechanical properties of base materials

Mechanical properties	σ_Y, MPa	σ_{UTS}, MPa	*E*, %
DC04 steel	160	280	37
6016-T4 alloy	140	260	28

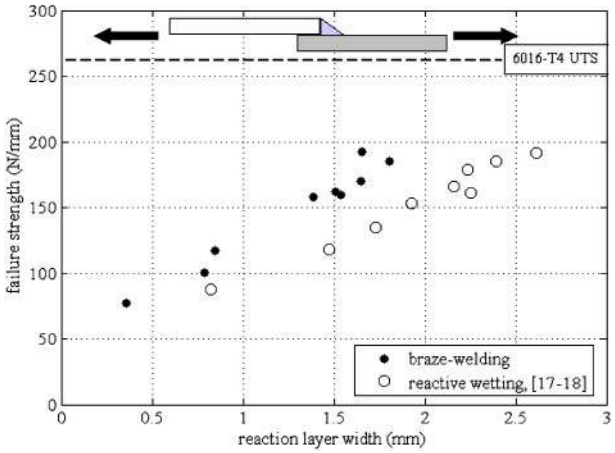

2 Failure strength versus reaction layer width for braze welded steel/Al assemblies and comparison with previous results obtained by reactive wetting[17,18]

melting of the filler wire and the Al sheet, which allows the bonding on the whole thickness of the Al sheet. In contrast, when the laser spot is directed only towards the filler wire (Fig. 4*b*), the Al sheet does not melt.

Macroscopic analysis of joints

The visual examination of the external surfaces of the beads did not reveal critical defects such as porosities or cracks. The wetting angle formed between solid steel and solidified Al decreases when the laser power increases, at constant filler wire and laser speeds (Fig. 3*b* and *c*), as previously observed by Saida,[16] revealing enhanced spreading of the melt pool. However, some scattering in the wetting angle along the bead is observed, and possibly explained either by changes in wire position versus laser irradiation, or by fluctuations in the wetting conditions during joining. The process analysis carried out by fast camera confirms this assumption. In Fig. 4*b*, successive images clearly show the change in steel surface wetting by liquid Al, which results in wetting angle modifications. The causes of these fluctuations may lie in the complex wetting mechanism of molten metals on solid substrates. This phenomenon is controlled by many factors, such as the interfacial temperature, the surface tensions, or the viscosity of the molten metal.[22–24] In the case of molten Al, another factor has a great influence: the formation of a thin oxide scale on the surface of the molten alloy. The spreading of Al on the substrate requires the elimination of the oxide layer, which is possible by the use of a flux. However, the dissolution of the oxide by the flux is not instantaneous. Lopez *et al*. have achieved *in situ* investigations on the action of a KAlF flux on the wetting of Al on a TiC substrate.[25] They observe that several seconds are required to dissolve Al_2O_3 at 900°C, and then to allow the spreading of molten Al on the substrate. The high laser speed (1 m min^{-1}), coupled to a rather inhomogeneous flux repartition on the surface, which could induce changes in the dissolution rate of the oxide, may then explain the variations of wetting angle observed. The roughness of the substrate surface also has an influence on the wetting.[23] However, the mechanical polishing of the surfaces with grade 800 SiC paper before assembling produces a homogeneous roughness on all the steel sheets.

If we now compare the average wetting angles obtained in braze welding with those obtained in previous reactive wetting tests with the same base

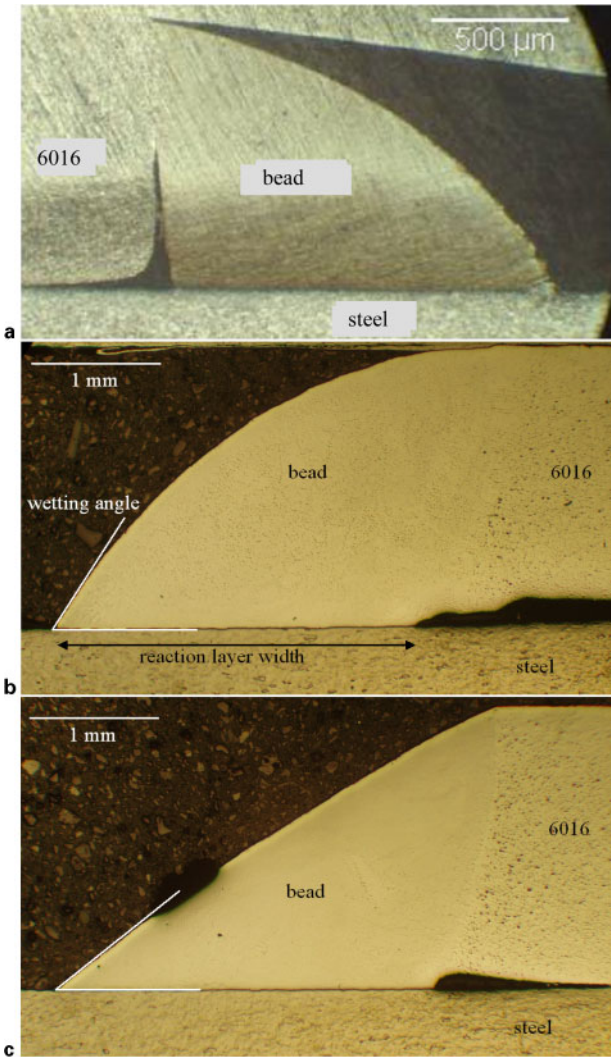

3 Cross-sections of bead, for *a* non-optimised laser spot location, *b* optimised laser spot location with *P*=2 kW and *c* optimised laser spot location with *P*=2·25 kW

materials,[17] the wetting angles in the present study seem slightly lower, for a similar linear energy (Fig. 5). These differences could be attributed to changes in the substrate temperature between reactive wetting and braze welding, or more probably to a change in the surface tension and/or in the viscosity of the molten zone. This last parameter is generally neglected, because the characteristic time to reach an equilibrium wetting angle (depending on the surface tensions) is very short, between 10^{-4} and 10^{-1} s according to the viscosity.[24] However in the authors' experiments, the scanning speed (16·7 mm s^{-1}) and the resulting thermal cycles could be too fast to reach the equilibrium wetting angle, and then the viscosity could have an influence. The presence of Si in the filler metal, which decreases the melting temperature of the alloy, could have an effect on the viscosity of the molten alloy and on its surface tension. Note that the wetting angles obtained by Saida[16] after braze welding with the same Al–12Si filler alloy, for similar linear energy, were slightly lower than the wetting angles of the present study. However, the laser speed was lower in the first study, allowing a better spreading of the filler metal, which could confirm the influence of the viscosity on the wetting angle.

The wetting is also dependent on the reaction layer formed at the interface, which generally increases the

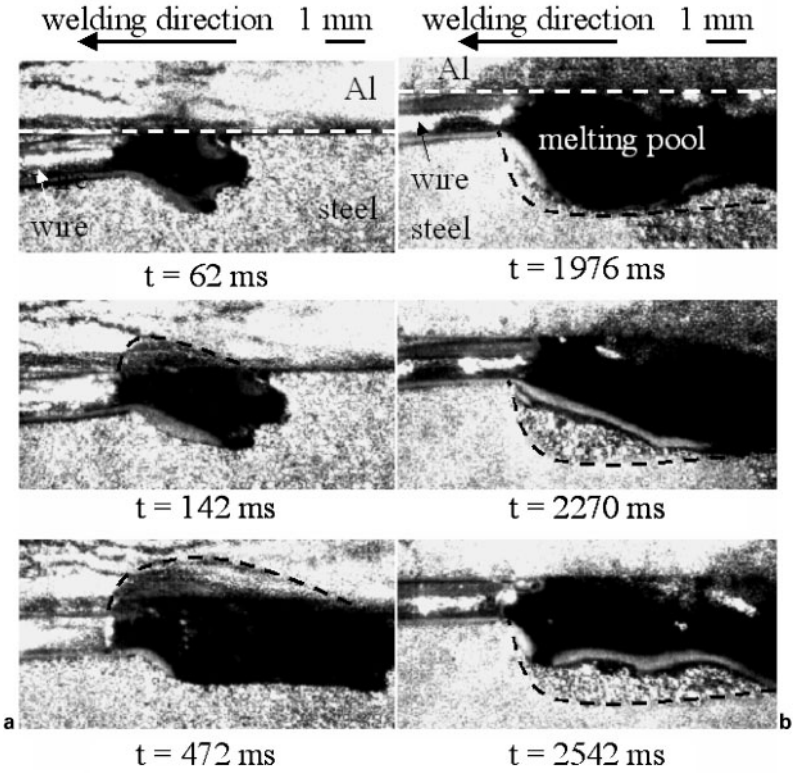

4 Fast camera video images showing *a* beginning of joining process with laser beam located on filler wire and 6016 sheet and *b* wetting issues in case of laser only located on filler wire

wetting angle in the case of Al/Fe wetting.[26] The high Si content in the filler wire could change the composition of the reaction layer compared to reactive wetting without filler metal, as already shown in a previous study,[17] and then modify the wetting angles.

The change in wetting angle also induces changes in bead width, which can reach up to 2 mm when the wetting angle decreases.

Microstructural analysis

Melted zone and 6016 bead joint

When the whole thickness of the 6016 alloy sheet is melted, a continuous joint is obtained between the parent Al alloy and the bead. During solidification, dendritic growth took place in the fusion zone with a particular orientation at the 6016 bead interface following the thermal gradient during cooling (Fig. 6). In contrast, equiaxed dendrites were observed in the centre of the bead, revealing higher solidification rate and/or lower thermal gradients at the end of the solidification. No Al oxide was observed between the bead and the parent Al alloy, as previously observed by Mathieu *et al.*[13] This later confirms the efficiency of the deposited flux.

The chemical analysis of the bead carried out with EPMA technique (Fig. 7) shows a rather homogeneous composition, with a 8 wt-%Si average content explained by the 4047 filler wire dilution occurring with the 6016 alloy. At a lower scale, microsegregation phenomenon is evidenced in the bead, resulting in the Mg and Si enrichment of the interdendritic zones. Iron was also detected in these locations, sometimes at a great distance

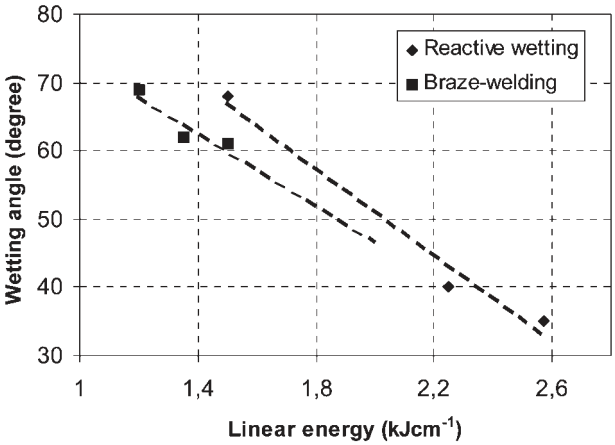

5 Comparison of wetting angles obtained in reactive wetting[17] and in braze welding

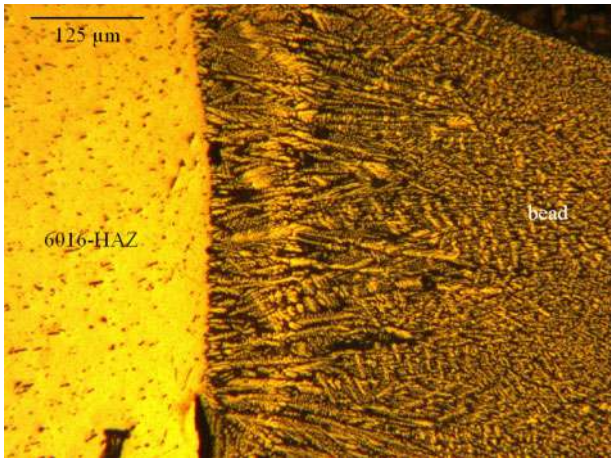

6 Cross-section of 6016 alloy/bead interface showing continuous bonding without apparent flaws

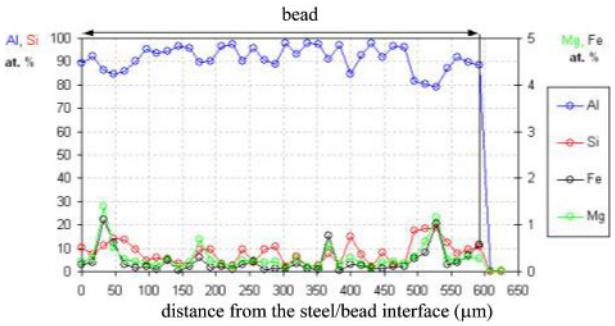

7 Chemical composition of bead (EPMA), at.-%

from the steel/bead interface (600 μm). Owing to the initial composition of the 4047 and 6016 alloys (0·2 and 0·5 wt-%Fe respectively), it was difficult to attribute the 0·5 wt-%Fe detected in the bead to a steel dissolution during joining,[18,26] even if the presence of Si in the melted Al is generally considered to favour Fe and intermetallic dissolution.[13,27] Some microporosity is also observed in the bead, close to the interface with steel (Fig. 8*a*). The presence of fluoride components in these areas, detected by EDX, seems to indicate that porosity is due to flux vaporisation. The bead root presents generally larger porosities, maybe due to trapped gas impeding the wetting of the brazing filler metal on the steel in these areas (Fig. 8*b*).

Bead/steel joint

Images of SEM reveal the formation of a very thin reaction layer at the interface between steel and bead. For the experimental parameters used in this study, the thickness of the layer was limited to 2 μm, and no cracks were evidenced. Most of the time, the reaction layer is rather uniform, and presents a flat interface in the steel side. In contrast, the reaction layer/bead interface presents an irregular aspect with some 'tongue-like' shape (Fig. 9) as already observed in previous studies on the solid steel to liquid Al interaction.[28] Some very fine needle-like precipitates are observed in the bead, close to the interface with steel. In some limited cases, larger intermetallic precipitates (Fig. 9*a*) were also evidenced close to the steel/bead interfaces in the centre area of the bead where the reaction layer is thicker. Owing to the low reaction layer thicknesses, correlations between the thickness and the experimental parameters (laser power, filler wire speed) could not be established.

If we compare these observations with previous results obtained by reactive wetting of 6016 on DC04 without filler metal,[17] the thickness of the reaction layer formed in the present study is rather lower, whereas the intermetallic precipitates in the bead are more numerous. This is in agreement with the general opinion that Si present in molten Al reduces the thickness of the reaction layer, by decreasing the diffusion rate of Al through the intermetallics layer, and by favouring the dissolution of the reaction layer in the melting pool, and then producing during cooling the precipitation of intermetallic phases in the melting zone.[10,27,29,30]

The chemical composition, determined by EDX, of the reaction layers and the intermetallic precipitates are rather similar (Fig. 9*a*). Nevertheless, due to the small size of the intermetallics (~1·5 μm for the reaction layer

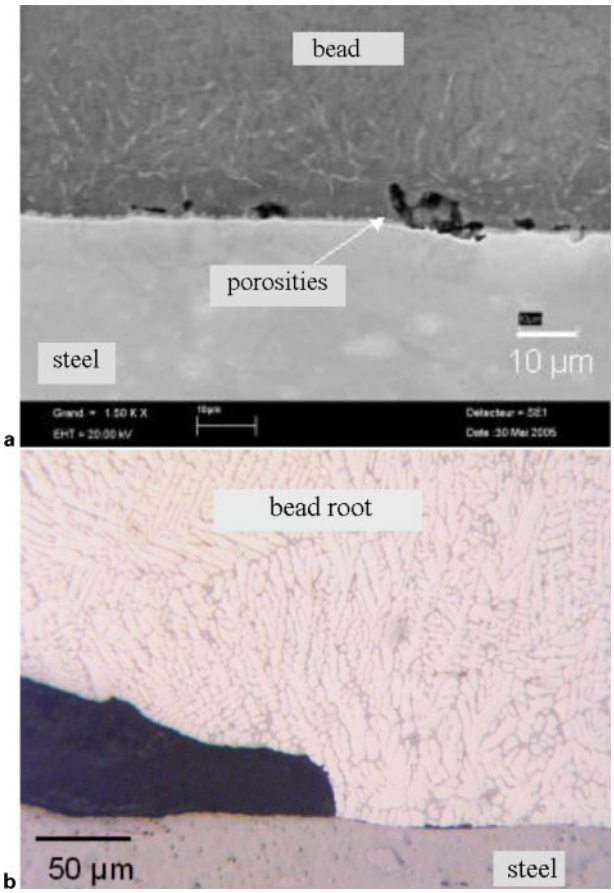

8 *a* microporosity at steel/bead interfaces due to flux vaporisation and *b* macroporosity at bead root due to trapped gas

thickness), the accuracy of this analysis is limited. The high Si content in the intermetallics seems however to suggest the formation of ternary intermetallic phases Fe–Al–Si.

Previous results obtained in reactive wetting of 6016 on DC04 have shown the main compound in the reaction layer was Fe_2Al_5, with a slight content of Si (1−2 wt-%),[17] but the $FeAl_3$ phase is also generally observed in the Al side.[10,27] In braze welding with 4047 filler alloy, the high Si content in the bead (8 wt-%) could modify the nature of the reaction layer. It has already been observed that an Fe–Al–Si intermetallic was formed at the liquid Al/solid steel interface when the melted Al contained more than 4 wt-%Si, whereas Fe–Al intermetalics were formed with lower Si contents.[10,27,30] In some recent works, several binary and ternary compounds formed in the Fe–Al–Si system were identified during interaction between steel and liquid Al–Si alloys: η-Fe_2Al_5, τ-$Al_{7,4}Fe_2Si$ and τ_6-$Al_{4,5}FeSi$,[29] or θ-$FeAl_3$, τ_5-$Al_{7,4}Fe_2Si$ and τ_{1-9}-$Al_3Fe_3Si_2$.[13]

The mechanisms of formation and growth of these intermetallic compounds were also discussed. It is generally accepted that the growth kinetic is controlled by two simultaneous phenomena: the diffusion controlled growth of intermetallic layers and its dissolution by molten alloy.[21,26,28,29] It is also well known that the presence of Si in the molten Al alloy enhances the dissolution.

According to Roulin *et al.*,[10] the first phase formed during furnace brazing of stainless steel with Al–12Si

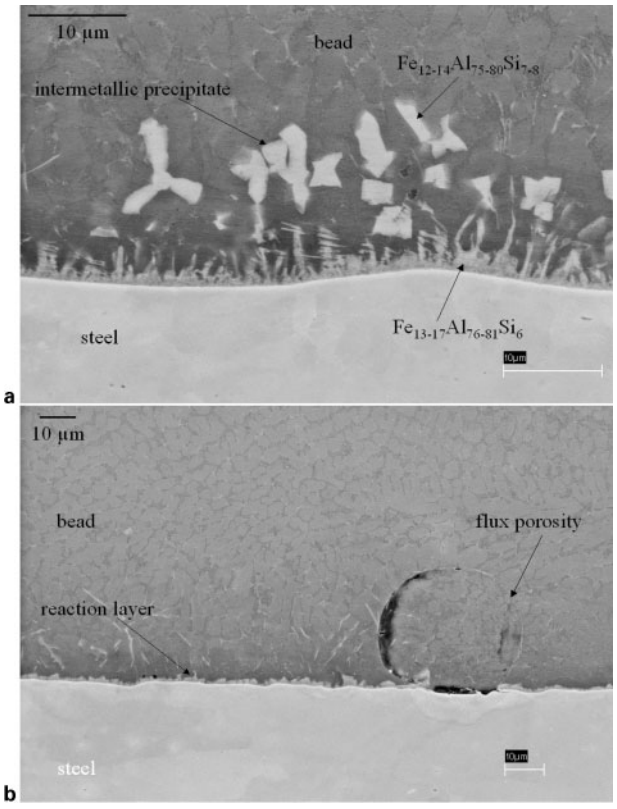

9 Cross-sections of steel/bead interfaces obtained by braze/welding with *P*=2 kW, showing reaction layer and intermetallic precipitates and non-bonding area due to porosity induced by flux vaporisation

filler metal at 600°C is a ternary Fe–Al–Si intermetallic, whereas a second Fe–Al intermetallic is formed at the Fe–Al–Si/steel interface for longer times. The parabolic growth of the first intermetallic layer, indicating a diffusion controlled mechanism, has revealed that for these bonding conditions, the dissolution of intermetallic was negligible. In contrast, according to Viala *et al.*,[29] the Fe–Al–Si intermetallic reaction layer formed at 780°C during hot dipping of steel in molten Al–7Si alloy remains very thin (2–3 μm) after 4 min. This stabilisation of the reaction layer thickness is attributed to its rapid dissolution. The dissolution rate of the intermetallic layer seems then to increase more rapidly with temperature than the diffusion rate through the reaction layer. However, the saturation of the molten pool by Fe stops the dissolution.

In the present study, the interaction between steel and molten Al alloy is very short (<1 s),[17] so it can be expected that the Al pool remains unsaturated. The maximum temperature reached at the steel/molten alloy interface, estimated by numerical simulation during reactive wetting,[17] is rather high, in the 800–1000°C range according to the linear energy employed.

From these data, the following mechanism can be proposed for the formation of the steel/bead bonding during weld brazing. During the heating cycle, the molten Al–Si alloy dissolves Fe, but also the formed intermetallic, due to the rapid temperature increase which favours the dissolution mechanism. In a second step, the cooling of the molten pool, from the interface towards the top of the pool, decreases the Fe solubility, and then induces the Fe–Al–Si intermetallic precipitation, first at the steel/pool interface, and then in the interior of the pool. The porosities induced by flux vaporisation (Fig. 9*b*), which appear before the formation of intermetallics, indicate the initial steel/pool interface. The growth of these phases can be seen to occur in the pool side, and not in the steel side, as observed when the intermetallic growth is diffusion controlled. This confirms the proposed mechanism.

Despite some uncertainty on the nature of the intermetallic phases, the brittleness of such compounds is obvious.[1–20] Peyre *et al.*[17] have already observed that some low amount of silicon in Fe_2Al_5 phase did not modify the hardness of this compound since identical values were obtained between phases containing up to 8 at.-%Si (1200 ± 100 $HV_{20\ mN}$) and 'pure' Fe_2Al_5.

Mechanical analysis of assemblies

A transverse tensile test, carried out with specimen width of 20 mm, is used to evaluate the mechanical properties of the steel/Al assemblies. As the configuration of the tensile specimen is not symmetrical (Fig. 2), a bending moment appears during the test,[31] when Al starts to deform plastically. Consequently the initial shearing stress state moved into a complex tensile shear stress applied to the reaction layer. That is why the mechanical strength of the assemblies is given in N mm^{-1} (failure strength divided by the specimen width) and not in MPa, due to the impossibility of separating tensile and shear stresses.

Failure strength of steel/Al assemblies

Two failure modes of the steel/Al assemblies are observed, either in the reaction layer, at the steel/bead interface (Fig. 10*a*) by a pure brittle mechanism, or by a mixed mode in the reaction layer and through the bead (Fig. 10*b*) according to a partially ductile mechanism. The corresponding failure strengths are in the 80–190 N mm^{-1} range, depending on the reaction layer width. The maximal failure strength represents ~73% of the ultimate tensile strength of the 6016-T4 alloy, which is in good agreement with the results obtained in the same configuration by Saida[16] (maximal failure strength of the assemblies ~76% of the ultimate tensile strength of the Al alloy). A very good correlation is observed between the failure strength and the reaction layer width, as shown in Fig. 2. The results obtained in the present study by braze welding are also close to the results obtained in the previous study by reactive wetting joining.[17,18] However, for a same reaction layer width, the braze welded steel/Al assemblies always seem to be more resistant, which could be explained by a change in the thickness and/or chemical composition of the reaction layers. The thicknesses obtained by reactive wetting were between 2 and 14 μm, higher than the reaction layer thicknesses obtained in the present study (<2 μm). This difference has been ascribed to the effect of Si in the melting pool, which enhances the intermetallic dissolution rate. A change was also observed in the chemical composition, since Fe_2Al_5 and possibly $FeAl_3$ phases, both containing some 1 wt-%Si, were identified in reactive wetting bonding, whereas Si richer phases are formed by braze welding due to the use of the Al–Si filler wire.

Even for the higher fracture strength (190 N mm^{-1}), the failure never occurs in the Al heat affected zone or at

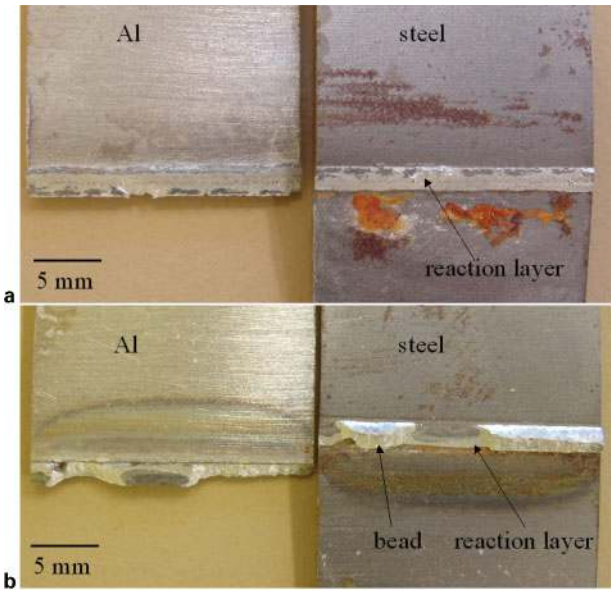

10 Macroscopic view of failure parts of assembly in case of *a* reaction layer failure and *b* mixed failure at reaction layer and through bead

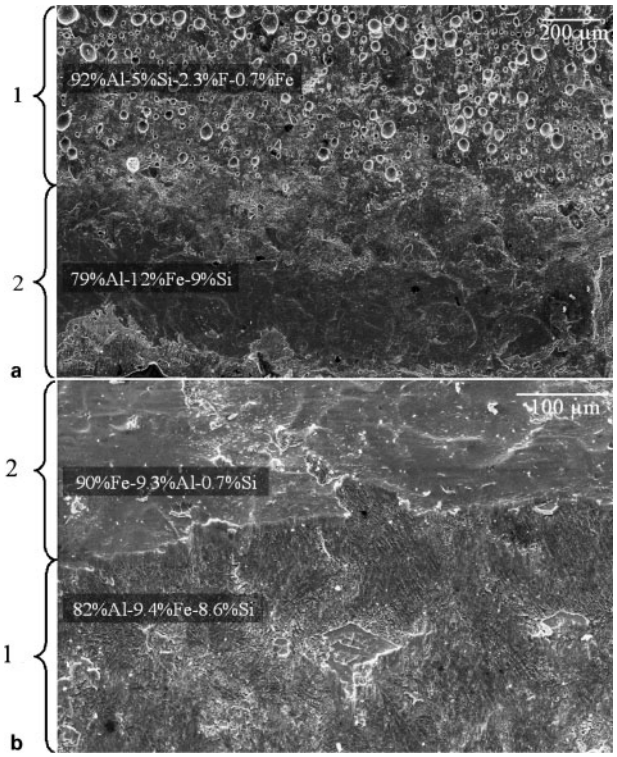

11 Images (SEM) of failed parts of assemblies on *a* Al side and *b* steel side

the Al/bead interface, in contrast to that previously observed in reactive wetting[18] or in braze welding with Zn–Al filler alloy.[14] The failure at the Al/bead interface was attributed to the occurrence of a liquation phenomenon in the case of reactive wetting, or to a Zn infiltration in the case of Zn–Al braze welding. These phenomena were not observed in the case of braze welding with Al–12Si filler wire.

If we compare the failure strength of samples obtained by lap braze welding with Zn–Al filler alloys[14] with the results of the present study, it seems that Al–12Si filler wire gives slightly better strength. Indeed, for similar bead width (~2 mm), the failure strength is ~73% of the ultimate tensile strength of 6016-T4 alloy with Al–12Si filler wire, versus ~65% with Zn–Al filler alloy.

Fracture analysis

For the failures occurring in the reaction layers, the SEM examination of the failed parts shows two different fracture patterns on each part of the failed samples (Fig. 11). Energy dispersive X-ray analysis of each zone allows to determine the crack path during the fracture. On the Al part of the fractured samples, on the bead root side (zone 1 in Fig. 11*a*), EDX analysis shows a composition rather close to the bead composition, but with a high F content, indicating the presence of crystallised flux components. On the opposite surface, on the steel part of the sample (zone 1 in Fig. 11*b*), the fracture pattern presents a dendritic aspect, and the EDX analysis reveals a very high Al content (82 at.-%), suggesting a fracture in the bead. The failure is then located, in the root area, in the bead close to the interfacial zone, which could be the weakest zone due to the presence of flux induced porosities. The external zone of the Al part, in the bead foot side (zone 2 in Fig. 11*a*) showed a significant difference in chemical composition (presence of Fe) and in failure aspect, showing flat surfaces which are characteristic of brittle failure in the intermetallic layer. The corresponding fracture pattern on the steel part (zone 2 in Fig. 11*b*) has a similar aspect, with a chemical composition richer in Fe, traducing a propagation either at the steel/reaction layer interface or in the intermetallic layer.

According to these observations the following fracture mechanism is proposed when the failure of the steel/Al assemblies occurs in the interfaces. The fracture initiation occurs at the bead root, where the stress concentration is maximal due to the root geometry, and propagates in the bead or at the bead/reaction layer interface, in the weakest zone containing flux induced porosities. Then, the failure is deflected and propagates in the reaction layer and/or at the steel/reaction layer interface.

Conclusions

Following previous works concerning the steel to Al joining by laser[12–18] or MIG process,[6,7] this study confirms that the dissimilar steel/Al joining is feasible. DC04 low carbon steel and 6016 Al alloy were joined by braze welding using a 4047 filler wire and a brazing flux. The joining was achieved by welding the 6016 parent alloy to the 4047 filler wire, and by brazing (reactive wetting) the liquid 4047 filler alloy to the solid steel.

The following major conclusions could be formulated.

1. Continuous bonds were obtained between the Al parent alloy and the Al–Si filler wire when the whole thickness of the initial sheet is melted.
2. Thin interfaces (<2 μm) of Fe–Al–Si intermetallics are generated between steel and bead.
3. Promising mechanical resistances were obtained (190 N mm^{-1}) not so far from the ultimate tensile strength of the lower parent material, i.e. the 6016-T4 alloy (260 N mm^{-1}). Most of the failures were located in the reaction layers, at the steel/bead interfaces.
4. The failure strength is directly related to the width of the layer.

Acknowledgements

The authors wish to thank F. Castilan and J. Grall from CEA/UTIAC Saclay for SEM EDX analyses and C. Merlet from University Montpellier II for EPMA analyses.

Thanks to Mrs Marshall for editing this manuscript.

The authors are grateful to Languedoc-Roussillon Region for financial support to this study.

References

1. J. H. Han, J. P. Ahn and M. C. Shin: *J. Mater. Sci*., 2003, **38**, 13–18.
2. S. Fukumoto, H. Tsubakino, K. Okita, M. Aritoshi and T. Tomita: *Mater. Sci. Technol*., 1999, **15**, 1080–1086.
3. G. Kawai, K. Ogawa, H. Ochi and H. Tokisue: *Weld. Int*., 2000, **14**, 101–107.
4. K. Kimapong and T. Watanabe: *Weld. J.*, 2004, **83**, 277–282.
5. H. Uzun, C. Dalle Donne, A. Argagnotto, T. Ghidini and C. Gambaro: *Mater. Design*, 2005, **26**, 41–46.
6. H. T. Zhang, J. C. Feng, P. He and H. Hackl: *Mater. Charact*., 2007, **58**, 588–592.
7. T. Murakami, K. Nakata, H. Tong and M. Ushio: *ISIJ Int*., 2003, **43**, 1596–1602.
8. M. Yasuyama, K. Ogawa and T. Taka: *Weld. Int*., 1996, **10**, 965–970.
9. X. Sun, E. V. Stephens, M. A. Khaleel, H. Shao and M. Kimchi: *Weld. J*., 2004, **83**, 188s–195s.
10. M. Roulin, J. W. Luster, G. Karadeniz and A. Mortensen: *Weld. J*., 1999, **78**, 151–155.
11. M. J. Rathod and M. Kutsuna: *Weld. J*., 2004, **83**, 16–26.
12. M. Kreimeyer, F. Wagner and G. Sepold: Proc. 23rd Int. Conf. on 'Applications of lasers and electro-optics', San-Francisco, CA, USA, October 2004, Laser Institute of America, CDROM.
13. A. Mathieu, S. Pontevicci, J.-C. Viala, E. Cicala, S. Mattei and D. Grevey: *Mater. Sci. Eng. A*, 2006, **A435–436**, 19–28.
14. A. Mathieu, R. Shabadi, A. Deschamps, M. Suery, S. Mattei, D. Grevey and E. Cicala: *Opt. Laser Technol*., 2007, **39**, 652–661.
15. H. Laukant, C. Wallmann, M. Muller, M. Korte, B. Stirn, H.-G. Haldenwanger and U. Glatzel: *Sci. Technol. Weld. Join.*, 2005, **10**, 219–226.
16. K. Saida, W. Song and K. Nishimoto: *Sci. Technol. Weld. Join*., 2005, **10**, 227–235.
17. P. Peyre, G. Sierra, F. Deschaux-Beaume, D. Stuart and G. Fras: *Mater. Sci. Eng. A*, 2007, **A444**, 327–338.
18. G. Sierra: 'Metallurgical and mechanical study of the steel to aluminium assembly by laser and GTAW processes', PhD thesis, Montpellier, France, 2006.
19. S. Katayama: *Weld. Int*., 2004, **18**, 618–625.
20. G. Sierra, P. Peyre, F. Deschaux-Beaume, D. Stuart and G. Fras: *Mater. Sci. Eng. A*, 2007, **A447**, 197–208.
21. G. Eggeler, W. Auer and H. Kaesche: *J. Mater. Sci.*, 1986, **21**, 3348–3350.
22. F. Delannay, L. Froyen and A. Deruyttere: *J. Mater. Sci*., 1987, **22**, 1–16.
23. K. Landry, S. Kalogeropoulou and N. Eustathopoulos: *Mater. Sci. Eng. A*, 1998, **A254**, 99–111.
24. K. Landry and N. Eustathopoulos: *Acta Mater*., 1996, **44**, 3923–3932.
25. V. H. Lopez and A. R. Kennedy: *J. Coll. Int. Sci*., 2006, **298**, 356–362.
26. V. N. Yeremenko, Y. V. Natanzon and V. I. Dybkov: *J. Mater. Sci*., 1981, **16**, 1748–1756.
27. P. Vaillant and J. P. Petitet: *J. Mater. Sci*., 1995, **30**, 4659–4668.
28. K. Bouché, F. Barbier and A. Coulet: *Mater. Sci. Eng. A*, 1998, **A249**, 167–175.
29. J. C. Viala, M. Peronnet, F. Barbeau, F. Bosselet and J. Bouix: *Composites A*, 2002, **33A**, 1417–1420.
30. D. Pierre, F. Barbeau, M. Peronnet, F. Bosselet and J. C. Viala: *Defect Diffus. Forum*, 2001, **194–199**, 1593–1598.
31. M. Merklein, A. Giera and M. Geiger: *Steel Res. Int.*, 2005, **76**, 250–256.